input voltages that provide useful circuit operation. Figure 4 shows the measured return loss of a typical attenuator chip at 7 GHz. (Return loss is similar at other frequencies within the range of 7–18 GHz.) The lower left region represents the minimum loss state of the attenuator, with series HEMT on and shunt HEMT off. As V_2 is made less negative to increase the attenuation by the shunt HEMTs, V_1 must be made more negative to maintain low return loss. This is easily understood by considering that the behavior of the HEMT varistor ladder network is closely analogous to a resistive tee or pi network. To achieve very high attenuation, V_2 must be increased toward 0 V, whereas V_1 is kept relatively constant. This can also be understood by the resistor network analogy. Although high (> 50 dB) attenuation is achieved in this region, the phase error is large, in the tens of degrees. Low phase error can, however, be achieved, with the chip operated up to an attenuation of 20–30 dB.

Figures 5(a)–5(c) show the rf performance of a typical attenuator to this attenuation level. About 7 degrees *p-p* phase error is exhibited over the frequency range of 7–18 GHz up to a (relative) attenuation of 23 dB. Note, however, that at the highest attenuation level shown, the return loss is marginal. For the right series/shunt resistance balance to obtain good return loss as attenuation is increased in the 20–30-dB region, the resistance of the series HEMT must be monotonically increased as that of the shunt HEMT is decreased. However, the parasitic capacitance of the series HEMT now begins to be seen, introducing a positive phase shift relative to the low attenuation state. Thus, for a given attenuation, one combination of V_1 and V_2 provides optimum return loss, while a slightly different combination provides minimum relative phase error. Figures 6(a)–6(c) illustrate how V_1 and V_2 can be adjusted to make a trade-off between return loss and phase error.

IV. CONCLUSIONS

We have successfully demonstrated a broadband microwave HEMT attenuator. The circuit provides amplitude control with low phase error to a relative attenuation of 20–30 dB.

ACKNOWLEDGMENTS

The authors would like to thank D. Savage for test engineering assistance, H. Mulderink for test data processing, M. Biedenbender for HEMT layouts, K. Ngo for device models, L. Rowe for circuit design guidance, P-H. Liu for E beam lithography, and G. Fisk for wafer testing.

REFERENCES

1. Y. Tajima, T. Tsukii, R. Mozzi, E. Tong, L. Hanes, and B. Wrona, "GaAs Monolithic Wideband (2–18 GHz) Variable Attenuators," *1982 IEEE MTT Symposium Digest*, pp. 479–481.
2. Hiroshi Kondoh, "DC-50GHz MMIC Variable Attenuator with a 30dB Dynamic Range," *1988 IEEE MTT Symposium Digest*, pp. 499–503.
3. Horng Jye Sun and James Ewan, "A 2–18 GHz Monolithic Variable Attenuator Using Novel Triple-Gate MESFETs," *1990 IEEE MTT Symposium Digest*, pp. 777–780.
4. J. P. Starski and B. Albinsson, "An Absorptive Attenuator with Optimized Phase Response," *Proc. 14th European Microwave Conf.* (Liege, Belgium), Sept. 10–13, 1984, pp. 510–516.
5. Robert J. Baeten, T. Koryu Ishii, and James S. Hyde, "*p-i-n* Diode Attenuator with Small Phase Shift," *IEEE Trans. Microwave Theory Tech.*, Vol. 36, No. 4, pp. 789–711, April 1988.
6. G. Lizama, T. Andrade, and R. Benton, "1–6 GHz GaAs MMIC Linear Attenuator with Integral Drivers," *1987 IEEE Microwave and Millimeter-Wave Monolithic Circuits Symposium Digest*, pp. 105–107.

CCC 0895-2477/97

A GENERALIZED METHOD FOR CHARACTERIZING TWO-DIMENSIONAL SCATTERING PROBLEMS WITH SPECTRAL TECHNIQUES

H. Esteban[1], J. M. López[1], V. E. Boria[1], M. Baquero[1], and M. Ferrando[1]
[1]Department of Communications
Universidad Politechnica
Camino de Vera S/N
46071 Valencia, Spain

Received 22 July 1996

ABSTRACT: *A new method for characterizing two-dimensional metallic objects (scatterers) using spectral techniques is outlined. The physical optics method and the method of moments are compared in order to find the response of the scatterer. Several examples illustrate the ease with which one can find the scattered field by an object to any incidence with a unique matrix used as a transference function. © 1997 John Wiley & Sons, Inc.* Microwave Opt Technol Lett 14, 6–9, 1997.

Key words: *scatterer transference function; spectral techniques; physical optics; method of moments*

1. INTRODUCTION

The characterization of objects from an electromagnetic point of view with a matrix used as a transference function has been studied by several authors [1, 2]. This matrix makes the scattering problem of an object independent of its geometry, so that the transference function gives the spectrum of the scattered field by the object as a response to any incident spectrum. In [2] the transference function was used in order to characterize reflectors with incident and scattered reference planes. In this article a more general method with cylindrical incident and scattered reference systems is presented, valid for any type of scattering object. In addition, we have employed and compared both physical optics and the method of moments in the construction of the transference function.

2. THEORY: TRANSFERENCE FUNCTION

The transference function [1] is a matrix that gives the electric field scattered by the object in the presence of any incidence field. The incident ($\mathbf{E}^i$) and scattered ($\mathbf{E}^s$) field can be expressed as a series of incident and emergent cylindrical modes (spectral components) centered somewhere inside the object:

$$\mathbf{E}^i = \sum_{p=-N_I}^{N_I} i_p J_p(k\rho) e^{jp\phi}\hat{z}, \quad \mathbf{E}^s = \sum_{q=-N_D}^{N_D} c_q H_q^{(2)}(k\rho) e^{jq\phi}\hat{z}, \tag{1}$$

where p and q count for the pth and qth spectral component, and i_p and c_q are the weights for these components. We will not use the whole spectrum of the incident or scattered fields, but just the most contributory components, so that p and q will count from $-N_I$ to N_I and $-N_D$ to N_D, where N_I and N_D satisfy that $N_I > ka$, $N_D > ka$, a being the radius of the minimum circumference that contains the scatterer.

In order to construct the transference function we must find the response of the object to each spectral component of the incident field $J_p(k\rho)e^{jp\phi}$ separately, as

$$\sum_{q=-N_D}^{N_D} d_{qp} H_q^{(2)}(k\rho) e^{jq\phi}, \tag{2}$$

where d_{qp} is the weight of the qth spectral scattered component as a result of the pth incident spectral component. If we repeat this process with all the spectral incident components, we can form the transference matrix of the scatterer as

$$\underline{D} = \begin{bmatrix} d_{-N_D,-N_I} & d_{-N_D,-N_I+1} & \cdots & d_{-N_D,N_I} \\ d_{-N_D+1,-N_I} & d_{-N_D+1,-N_I+1} & \cdots & d_{-N_D+1,N_I} \\ \vdots & \vdots & \ddots & \vdots \\ d_{N_D,-N_I} & d_{N_D,-N_I+1} & \cdots & d_{N_D,N_I} \end{bmatrix}. \tag{3}$$

Once we have obtained this matrix, we have the scatterer fully characterized, so that for different incident electric fields (column vector $\underline{i_p}$), we know the scattered field (column vector c_q) by just multiplying our transference matrix $\underline{D}$ by the column vector of weights $\underline{i_p}$. This technique allows us to forget about the scatterer and just use its transference function, which is the only information we need.

3. CONSTRUCTION OF THE TRANSFERENCE FUNCTION

The computation of the transference matrix includes four steps:

1. Suppose the incident field is one of the cylindrical modes $J_p(k\rho)e^{jp\phi}$.
2. Find the current density $\mathbf{J}_s$ excited on the object surface with the use of some classical analysis methods, such as physical optics (PO) or the numeric method of moments (MoM).
3. Express the scattered field produced by $\mathbf{J}_s$ in terms of a series of emergent cylindrical modes with the addition theorem of Bessel functions. That series will be the pth column of the transference function.
4. Repeat the process by running p from $-N_I$ to N_I.

In the second step we have used both the MoM and the PO method. In the latter the current density $\mathbf{J}_s$ on the scatterer surface is determined from the well-known approximation $\mathbf{J}_s = 2[\mathbf{n} \times \mathbf{H}^i]$. In this case we must transform the incident field cylindrical spectrum into a plane-wave spectrum [3], so that the current excited by each plane-wave mode (incidence angle β) is $2[\mathbf{n} \times \mathbf{H}^i]$ only on the illuminated areas of the surface of the object.

In the MoM [4] we do not need to transform the spectrum into a planar one. We choose pulse functions as base functions and deltas as testing functions (point-matching method), and then we find the current density $\mathbf{J}_s$ on certain sampled points of the surface.

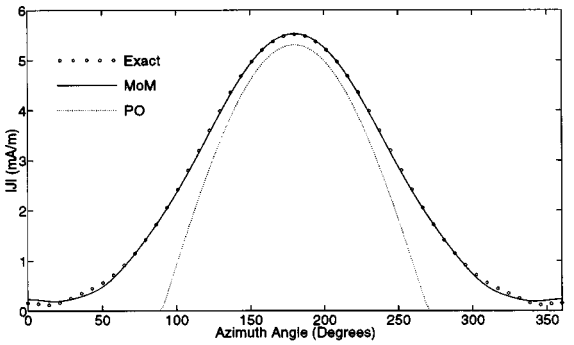

Figure 1 Amplitude of the surface current density $\mathbf{J}_s$ in a 0.5λ-radius cylinder with plane-wave incidence. Comparison of the physical optics method, the method of moments, and the exact solution

The current density $\mathbf{J}_s$ induced by an incident plane wave $E_z^i = e^{-jk\rho\cos(\phi-\beta)}$, with $\beta = 0$ (plane wave incises from negative X semiaxis) on the surface of a 0.5λ-radius cylinder is shown in Figure 1. We observe that for small scatterers in terms of the wavelength the method of moments is more accurate than the physical optics method, especially as the induced current on the shaded surface of the cylinder ($-90° < \phi < 90°$) is not too small, whereas in the physical optics approximation it is considered to be zero. Even on $90° < \phi < 270°$ the PO approximation is shown to be inadequate. Therefore, the physical optics method is not viable with small objects, as is widely known, and the method of moments is more suitable, giving a good solution for $\mathbf{J}_s$ on the whole surface of the scatterer. We can see in Figure 2, however, that as the size of the scatterer increases, the density $\mathbf{J}_s$ on the shaded surface decreases and the accuracy of the physical optics method gradually approaches that of MoM also on $90° < \phi < 270°$. Furthermore, the PO method gives $\mathbf{J}_s$ analytically and its computation is immediate, whereas in the method of moments the numerical process requires an increasing computational effort as the object size increases. Consequently, the physical optics method is a good alternative to the MoM when the scatterer is large, for it is extremely fast and gives an exact solution in the front semispace, and a good approximation in the back semispace with a plane-wave incidence.

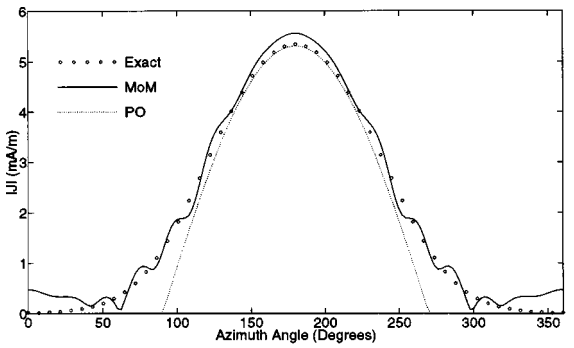

Figure 2 Amplitude of the surface current density $\mathbf{J}_s$ in a 1.5λ-radius cylinder with plane-wave incidence. Comparison of the physical optics method, the method of moments, and the exact solution

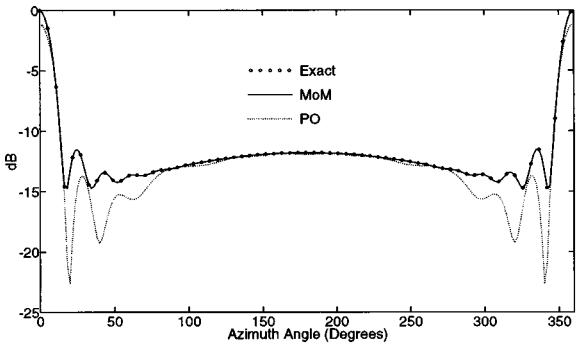

Figure 3 Comparison of the physical optics method, the method of moments, and the exact data. Scattered field by a cylinder (radius 1.5λ) when the incident field is a plane wave ($\beta = 0°$)

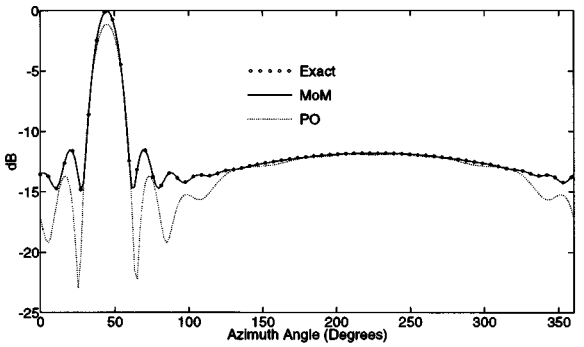

Figure 4 Comparison of the physical optics method, the method of moments, and the exact data. Scattered field by a cylinder (radius 1.5λ) when the incident field is a plane wave ($\beta = 45°$)

When the matrix $\underline{D}$ for a scatterer is formed, we can compute the scattered field immediately because of several incident waves. In Figures 3 and 4 the scattered field of a cylinder of 1.5λ radius is depicted, due to a plane-wave incidence ($\beta = 0°$ and $\beta = 45°$). The exact field is also represented [5]. To compute this, we have formed the transference function with the use of both the MoM and the PO method. The scattered field has a peak for $\phi = 0$ when $\beta = 0$. That peak produces a shade behind the cylinder when added to the incident plane wave. This peak moves to $\phi = 45°$ when $\beta = 45°$, as was expected. We also notice that the MoM gives very precise results in the whole space, whereas the PO method is more accurate in the front semispace ($90° < \phi < 270°$) than in the back one ($-90° < \phi < 90°$). The accuracy of the PO approximation increases as the scatterer electrical dimension increases.

4. RESULTS

A parabolic reflector ($f = 3\lambda,\ D = 5\lambda$) has been used to obtain simulation results. Its transference function has been computed with the MoM. By using the very same matrix, we have obtained the response of this parabolic reflector when two different fields fall upon its surface. In Figure 5 the phase of the scattered field is depicted when a line source is at focus. We observe that the phase in the front semispace is plane, as was expected. In the back semispace the phase corresponds to a cylindrical wave centered at focus but shifted 180° from that of the incident wave, so that the total field is zero, forming the shade of the reflector. The line source has been placed $\lambda/2$ over the focus in Figure 6. The reflected

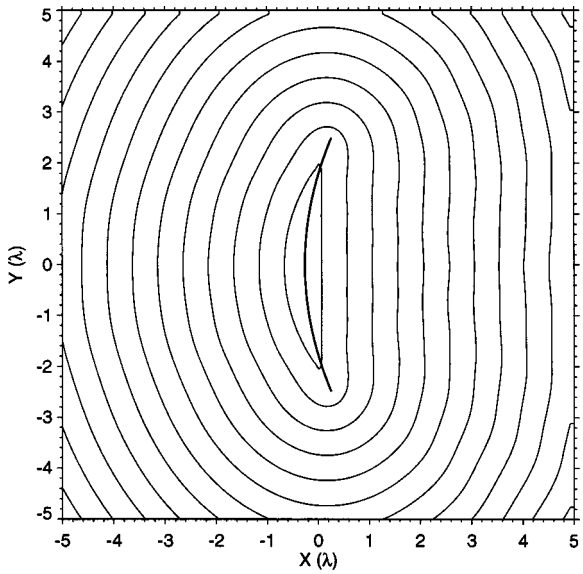

Figure 5 Phase of scattered field by a parabolic reflector ($f = 3\lambda$, $D = 5\lambda$) with a line source at focus

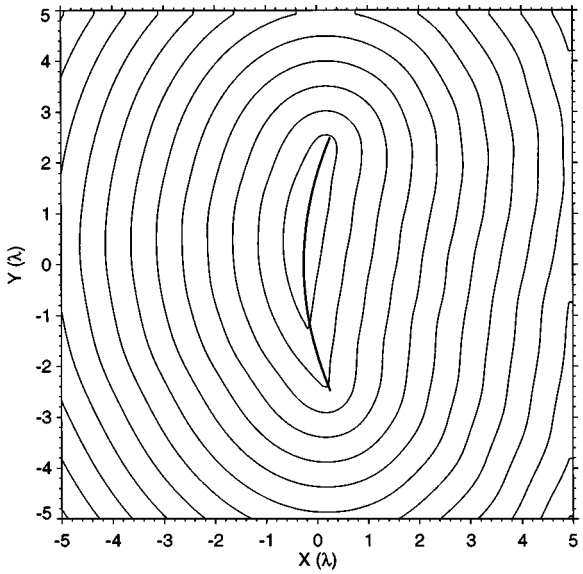

Figure 6 Phase of the scattered field by a parabolic reflector ($f = 3\lambda$, $D = 5\lambda$) with a line source $\lambda/2$ over the focus

phase shows that the direction of the phase front is slanted. The scattered field depicted in Figures 5 and 6 has been calculated in two different ways. In the region outside the cylinder that contains the object we have used the transference function, and inside this cylinder the field has been determined by the integration of the excited current $\mathbf{J}_s$ [1], for the scattered field spectrum is only valid in regions without sources.

5. CONCLUSIONS

As a conclusion we emphasize that this method makes the calculation of the scattered field by the same object independent from the nature of the incident field, once we have obtained its transference matrix. Moreover, this calculation consists of a simple matrix multiplication. Finally we outline

the analysis of multiple scatterer problems as a direct application of the method.

REFERENCES

1. J. C. Cruellas, "Análisis de la Difracción de Objetos Dieléctricos Mediante Elementos Finitos y Realimentación Modal," Ph.D. thesis, Universidad Politécnica de Cataluña, Barcelona, 1989.
2. V. E. Boria, M. Baquero, and M. Ferrando, "Analysis of Multireflector Antenna Clusters by Spectral Methods," *24 European Microwave Conference*, Cannes, Sept. 1994, Vol. 1, pp. 870–875.
3. M. Baquero, "Transformaciones Espectrales y Aplicaciones a Síntesis de Ondas, Medida de Antenas y Difracción," Ph.D. thesis, Universidad Politécnica de Valencia, Valencia, 1994.
4. R. F. Harrington, *Field Computation by Moment Method*, The Macmillan Company, New York, 1968.
5. C. A. Balanis, *Advanced Engineering Electromagnetics*, John Wiley & Sons Inc., New York, 1989.

CCC 0895-2477/97

THE EVALUATION OF MFIE INTEGRALS WITH THE USE OF VECTOR TRIANGLE BASIS FUNCTIONS

R. E. Hodges[1] and Y. Rahmat-Samii[1]
[1]Department of Electrical Engineering
University of California, Los Angeles
Los Angeles, CA 90095

Received 17 July 1996

ABSTRACT: *Formulas that provide an efficient and reliable numerical evaluation of the magnetic field integral equation (MFIE) with the use of vector triangular basis functions are developed. The MFIE integrals for the three basis functions on a triangular facet are converted from three vector integrals to three scalar integrals, which are evaluated simultaneously. The $1/R^2$ singular behavior is extracted from the integral, and closed-form expressions are given for the singular terms. Consequently, the formulas are valid for all observation points and are suitable for general-purpose modeling. © 1997 John Wiley & Sons, Inc.* Microwave Opt Technol Lett 14, 9–14, 1997.

Key words: *magnetic field integral equation (MFIE); triangular basis functions; singularity; scattering*

I. INTRODUCTION

Electromagnetic radiation and scattering problems formulated in terms of the electric field integral equation (EFIE) are frequently solved by the moment method [1]. A key element of moment-method analysis is the choice of basis functions used to represent the equivalent surface current of a physical object. The basis functions determine the physical geometry that can be represented and strongly influence computational costs. In order to model complex three-dimensional metallic objects found in typical engineering applications, one needs basis functions that can describe an arbitrarily shaped sheet of surface current **J** with a minimum number of unknowns. Vector basis functions [2] and a triangular surface patch model are widely used for this purpose. Because there is one unknown per edge, for a large mesh there are only ~ 1.5 unknowns per triangle. Consequently, these basis functions are attractive because they provide a very economical way to represent **J**.

Contract grant sponsor: Lockheed Advanced Development Company.

An important aspect of the computational cost is the time required to fill the moment-method matrix. The EFIE matrix elements for a perfect conductor require one to evaluate the integral representation of magnetic vector potential **A** and electric scalar potential Φ over an arbitrarily shaped triangular facet. Efficient and numerically stable methods have been developed to evaluate these integrals [2, 3]. In particular, a total of three scalar numerical integrations are needed on each triangular facet to compute both **A** and Φ.

More recently, the vector basis functions have been used to solve the magnetic field integral equation (MFIE) [4] and also to evaluate the physical optics integral [5, 6]. The MFIE integral introduces additional difficulties that do not appear in the corresponding EFIE integrals because of the presence of a cross product with the gradient of the Green's function in the integrand. A brute force evaluation of the cross product is inefficient and therefore limits the usefulness of the vector basis functions. Furthermore, the MFIE integral contains a $1/R^2$ singularity that leads to numerical problems for observation points in the vicinity of a source point. This article provides a mathematical construction that permits efficient and reliable evaluation of the MFIE integrals. Specifically, the MFIE integral is reduced to a form that requires only three scalar numerical integrations. In addition, closed-form analytic expressions are given for the singular part of the integral.

II. THE MFIE INTEGRAL ON A TRIANGULAR FACET

The MFIE for a closed conducting body can be expressed [7] as

$$\mathbf{J}(\mathbf{r}) = 2\hat{n} \times \mathbf{H}^{\text{inc}}(\mathbf{r}) + 2\hat{n} \times \oint_S \mathbf{J}(\mathbf{r}') \times [\nabla' G(\mathbf{r}, \mathbf{r}')]\, dS', \tag{1}$$

where $\mathbf{J}(\mathbf{r}')$ is the surface current density, $\mathbf{H}^{\text{inc}}$ is the incident magnetic field, $\hat{n}$ is a unit outward normal, the free-space Green's function is $G = e^{-jkR}/4\pi R$, $R = |\mathbf{r} - \mathbf{r}'|$ is the distance between observation point $\mathbf{r}$ and source point $\mathbf{r}'$, and $k = 2\pi/\lambda$, with λ the wavelength. Our focus is on the integral on the right in (1), which represents the scattered magnetic field $\mathbf{H}^s(\mathbf{r})$. It is convenient to write $\nabla' G$ in the form

$$\nabla' G(\mathbf{r}, \mathbf{r}') = \left(jk + \frac{1}{R} \right) \frac{e^{-jkR}}{4\pi R} \hat{\mathbf{R}}, \tag{2}$$

with $\mathbf{R} = \mathbf{r} - \mathbf{r}'$ and $\hat{\mathbf{R}} = \mathbf{R}/R$. This identity permits the scattered magnetic field integral in (1) to be written

$$\mathbf{H}^s(\mathbf{r}) = -\frac{1}{4\pi} \oint_S \left(jk + \frac{1}{R} \right) \hat{\mathbf{R}} \times \mathbf{J}(\mathbf{r}') \frac{e^{-jkR}}{R}\, dS'. \tag{3}$$

We seek to evaluate this integral for the case when **J** is expanded in terms of vector triangular basis functions [2] defined by

$$\mathbf{f}_n^{\pm}(\mathbf{r}) = \frac{\boldsymbol{\rho}^{\pm}}{2A_n^{\pm}}, \qquad \mathbf{r} \in S_n^{\pm}. \tag{4}$$